

COVER PAGE

Document downloaded by @DAEL

Thu Nov 19 23:02:40 2026
For personal use

When automatic English translation is provided, only the original document is authentic.
The EAA cannot be held responsible of any translation error

Bibliographical reference

A Model for Turbulent Combustion Noise, J. Wäsle, A. Winkler, F. Weyermann, C. Hirsch and T. Sattelmayer, Acta Acustica **vol. 95** (Number 3), 2009, pp. 391-401

DOI
https://doi.org/10.3813/AAA.918163

ACTA ACUSTICA UNITED WITH ACUSTICA
Vol. 95 (2009) 391 – 401

Scientific Papers
DOI 10.3813/AAA.918163

A Model for Turbulent Combustion Noise

J. Wäsle, A. Winkler, F. Weyermann, C. Hirsch, T. Sattelmayer
Technische Universität München, Lehrstuhl Thermodynamik, Boltzmannstrasse 15, 85747 Garching, Germany.
hirsch@td.mw.tum.de

Summary
We validate a spectral model for the fluctuating heat release rate of turbulent premixed flames which can be used in the source term of the acoustical wave equation to calculate the noise emission of turbulent combustion devices. The model is based on an assumed Eulerian model spectrum of progress variable, on a turbulent combustion model and on a space time mapping which allows to transform the spatial spectrum into a temporal spectrum needed for the acoustical wave equation. The details and the overall performance of the model were validated experimentally on premixed swirling jet flames using optical and acoustical measurement techniques, which are explained in the paper. The comparison is very good suggesting that the model can be applied in the engineering practice which is demonstrated on two examples.

PACS no. 4328.Kt

1. Introduction

Over the last years turbulent combustion noise has become a focus of interest in industrial gas turbines, jet engines and domestic water heaters in order to optimize designs for durability and minimal sound emission. The fundamental connection between the turbulent reactive flow field and the generation of sound is known since the pioneering work of Lighthill [1] in 1952. There its mathematical description emerged as a by-product of the analysis of aerodynamically generated noise which most of the early theoretical and experimental work was focused on [2, 3]. Almost a decade later the first studies on combustion generated noise were published [4, 5, 6]. While most authors in the field of combustion noise agree that the coherent heat release structures postulated by Strahle [5] determine the overall noise emission of the investigated flames the spectral behavior was hardly considered [6, 5, 7, 8]. In the early 90s Clavin [9] proposed a connection between the turbulent flow field and the noise emission of turbulent flames, that exhibited a reasonable amplitude decay according to an exponential power law but could not provide a quantitative closure for sound pressure levels. Boineau *et al.* [10] analyzed turbulent diffusion flames with spatial coherence functions arriving at a model for the sound spectrum which was able to reproduce the measured spectral behavior. Klein and Kok [11, 12] proposed a formal closure for calculating sound pressure from turbulent diffusion flames based on local mean turbulence, mean reaction rate density and an assumed model spectrum for heat release fluctuation. However, it relied on the specification of an empirical coherence length scale to calibrate the model. Also the space time mapping proved to be non-universal. The model for turbulent premixed flames proposed by Hirsch *et al.* [13] was shown to provide quantitative spectra of acoustic power based on local mean turbulence and heat release rate density without adjustments. Their theory provides a local spatial model spectrum of heat release rate fluctuation from mean quantities and the mapping of the spatial spectrum to the temporal spectrum needed for the calculation of the sound pressure frequency spectrum. With this model the thermo-acoustic source term of the wave equation (as shown in e.g. Crighton *et al.* [14]) can be evaluated allowing the calculation of the turbulent combustion noise spectrum for an acoustic system, e.g. by a Finite Element method or acoustical network analysis. For free space an analytical solution exists, which is used below in the validation experiments. Recently a new approach has been published by Mühlbauer *et al.* [15] that uses an assumed shape spatio-temporal correlation function which is fed with local turbulence data and the distribution of the temperature variance from a RANS calculation. Using stochastic forcing temporal acoustic source terms can be calculated which feed an aero-acoustics code to calculate the sound propagation with good comparison to experimental data.

In this paper first the model presented by Hirsch *et al.* [13] is outlined. Then the experimental setup and methods used to validate the model are shown, followed by the comparison of experimental and model data. Finally two practical examples are given for the model application.

Received 5 June 2008,
accepted 21 January 2009.

2. Theory

For sufficiently large turbulence Reynolds-number $Re_t = u' \cdot l_t / a_0$, a_0 being the thermal diffusivity, and requiring that the turbulence velocity u' and turbulence integral length scale l_t are sufficiently larger than the laminar flame

© S. Hirzel Verlag · EAA

Document downloaded by @DAEL, 2026-11-19 23:02:43 - personal use only

speed s_l, $u'/s_l > 1$ and the laminar flame thickness δ_l, $\delta_l/l_t \approx a_0/(s_l \cdot l_t) << 1$, the mean heat release rate density $\tilde{q}$ ($[W/m^3]$) can be expressed as a function of the mean scalar dissipation rate $\tilde{\xi}_{c^2}$ of the variance of the progress variable $\tilde{c'^2}$ [16] and is modeled formally as the dissipation rate of a passive, diffusive scalar, where $\epsilon \approx u'^3/l_t$ is the dissipation rate of turbulence kinetic energy $k = 1.5u'^2$, both per unit mass.

$$\tilde{q} = \rho_0 \, Y_{F,0} \, H_u \, \tilde{\xi}_{c^2} = \rho_0 \, Y_{F,0} \, H_u \cdot C_D \frac{\epsilon}{k} \tilde{c'^2} \tag{1}$$

with $C_D = 2.0$ being a model constant of the scalar dissipation model as proposed in [16]. ρ_0, $Y_{F,0}$ and H_u are the reactant density, fuel mass fraction and lower heating value respectively. For simplicity it is assumed that the thermal diffusivity of the fresh mixture a_0 be equal to the kinematic viscosity, i.e. $Pr = 1$. Equation (1) suggests that the spectrum of heat release can be obtained if the spectrum of $\tilde{c'^2}$ were known, thus:

$$\tilde{E}_q = \rho_0 \, Y_{F,0} \, H_u C_D \frac{\epsilon}{k} \tilde{E}_{c^2}. \tag{2}$$

Assuming for the moment that c behaves as a passive scalar, one may use the model spectra derived by Tennekes and Lumley [17] with their proposed constants $\alpha = 1.5$, $\beta = 0.3$. After some algebra one obtains

$$\begin{aligned} \tilde{E}_q &= \tilde{q} \cdot \frac{C_s \cdot C_D}{\alpha} \cdot \alpha \, \frac{\epsilon^{2/3}}{k} \, \kappa^{-5/3} \\ &\quad \cdot \exp\left[-\frac{3}{2} \left(\pi \beta \alpha^{1/2} \, (\kappa l_t)^{-4/3} + \alpha \, (\kappa \eta_{c^2})^{4/3} \right) \right] \\ &= \tilde{q} \cdot \frac{C_s \cdot C_D}{\alpha} \frac{E_{u^2}}{k}, \end{aligned} \tag{3}$$

where C_s is an amplitude scaling function which is derived further below. In the limit of large turbulent Damköhler number $Da_t \to \infty$ this function must have the value $C_s(Da_t \to \infty) = \alpha/C_D$ to be consistent with the scalar dissipation model equation (1). E_{u^2} is the turbulence kinetic energy spectral density as e.g. proposed by Tennekes and Lumley [17] of which the integral over all wavenumbers is the turbulence kinetic energy k. η_{c^2} is the Corrsin / Kolmogorov scale, which for the passive scalar becomes $L_C = (a_0^3/\epsilon)^{0.25}$. To include the effect of c not being a passive scalar Hirsch *et al.* [13] consider two effects:

The propagation speed of the flame front characterized by the Gibson scale $L_G = s_l^3/\epsilon$ which will tend to "iron out"the small scales, i.e. produce a spectral cut off at high wavenumber. They propose to consider it through an effective Corrsin scale:

$$\eta_{c^2} = \max\left[c_G L_G, L_C \right] \quad \text{with} \quad c_G = 3.0. \tag{4}$$

The change of flame regime. With decreasing Damköhler number or increasing Karlovitz number a decrease in spectral amplitude is expected due to the effects of finite rate chemistry which reduce the variance of the progress variable $\tilde{c'^2}$ [18, 16].

Reducing the variance corresponds to scaling the peak amplitude of the power spectrum, since the spectral cut-off is already considered. Hirsch *et al.* use the average heat release density model proposed by Schmid *et al.* [19]

$$\begin{aligned} \tilde{q} &= 4.96 \frac{\epsilon}{k} \tilde{c} \, (1 - \tilde{c}) \\ &\quad \cdot \left(\frac{s_l}{\sqrt{2/3 \, k}} + \left(1 + Da_t^{-2} \right)^{-0.25} \right)^2 \cdot \rho_0 \, Y_{F,0} \, H_u, \end{aligned} \tag{5}$$

$$Da_t = \frac{0.09 \cdot k \cdot s_l^2}{\epsilon \cdot C_c^2 a_0}, \tag{6}$$

where is a model constant from the Schmid model with $C_c \approx 1.2$ for Natural Gas fuel. Comparing the terms of equation (5) for a given finite Damköhler number with those for large Damköhler number Hirsch *et al.* derive a scaling function for C_s in equation (3) which is

$$\begin{aligned} C_s &= \frac{\alpha}{C_D} \frac{\tilde{c'^2}\left(Da_t\right)}{\tilde{c'^2}\left(Da_t \to \infty\right)} \\ &= \frac{\alpha}{C_D} \left(\frac{\frac{s_l}{\sqrt{2/3 \, k}} + \left(1 + Da_t^{-2} \right)^{-0.25}}{\frac{s_l}{\sqrt{2/3 \, k}} + 1} \right)^2. \end{aligned} \tag{7}$$

With this scaling function the necessary asymtotic behaviour of the heat release spectrum is obtained, since $C_s \to 0$ for $Da_t \to 0$, i.e. the homogeneous reactor limit, where no heat release fluctuations exist. Up to here the model determines the local wavenumber spectrum of heat release density based on average quantities by inserting equations (7) and (4) into equation (3).

To obtain the temporal spectrum $\psi(2\pi f)$ from the spatial spectrum $E(\kappa)$ Hirsch *et al.* follow Tennekes and Lumley [17] by requiring that the spectral energy content of corresponding scales is conserved, i.e. $\kappa E = 2\pi f \psi$ and postulating that the Lagrangian spectrum is a simple rearrangement of the Eulerian spectrum. For homogeneous turbulence this gives the following mapping between wavenumber and frequency.

$$\kappa = \frac{2\pi}{l_t} \cdot \frac{(2\pi)^{0.5}}{\alpha^{0.75}} \cdot \left(f \tau_c \right)^{1.5}. \tag{8}$$

Here $\tau_c = l_t/u'$ is the characteristic time scale. In premixed turbulent combustion this time scale is given by the passing time of the large scales through the flame brush, i.e. the ratio of the flame brush thickness δ_t and the turbulent burning speed s_t: $\tau_c = C_\tau \delta_t / s_t$. Using the turbulent burning velocity relations also proposed by Schmid, Hirsch *et al.* obtain:

$$\tau_c = C_\tau \cdot \frac{\delta_t}{s_t} = C_\tau \cdot \frac{l_t}{u'} \cdot \frac{a_0/(s_l \cdot l_t) + \left(1 + Da_t^{-2} \right)^{0.25}}{s_l/u' + \left(1 + Da_t^{-2} \right)^{-0.25}}, \tag{9}$$

with $C_\tau \approx 0.5$.

Given the local frequency spectra of heat release density $\psi_q = \kappa E_q/(2\pi f)$ by combining equations (3), (4), (7),

Document downloaded by @DAEL, 2026-11-19 23:02:43 - personal use only

(8) and (9) the frequency spectrum of the acoustic power in free space can be computed according to e.g. Winkler *et al.* [20]. For this the correlation spectrum of the partial derivative of the heat release with respect to time needs to be integrated over the flame volume V_f. As shown in Wäsle [21] this amounts to integrating the contributions from the coherent monopole sources with a correlation volume $V_{coh} = 8\, l_{coh}^3$ over the flame volume. The coherence length scale is evidently $l_{coh} = \delta_t$, which is confirmed by experimental findings [8].

$$P_{ac} = \frac{2\pi}{4\pi\rho_0 c_0}\left(\frac{\gamma-1}{c_0^2}\right)^2 \cdot \int_{(V_f)} (2\pi f)^2 \left(\frac{\kappa E_q(\kappa)}{2\pi f}\right)^2 \cdot 8 \cdot \left(\delta_t\right)^3 \mathrm{d}V_f \quad \left[\mathrm{W/Hz}\right]. \tag{10}$$

3. Experimental setup and methods

Validation experiments were carried out on premixed swirling jet flames generated by a generic swirl burner shown in Figure 1 operating on natural gas (NG) and NG/H_2 mixtures with air. It consists of a radial swirler with an annular nozzle having inner and outer diameters of $d = 16$ mm and $D = 40$ mm. Blocking the swirler slots to a selected length l_{eff} the swirl strength can be varied. In the experiments thermal power was varied between $\dot{Q}_{\mathrm{th}} = 30$–$90$ kW, equivalence ratio was in the range $\Phi = 0.71$–1 and swirl numbers were $S = 0$–0.6.

$$S = \frac{\int_{(\dot{m})} w \cdot r\, \rho u \,\mathrm{dA}}{\int_{(\dot{m})} \rho u^2 \,\mathrm{dA} \cdot D/2}, \tag{11}$$

where u, w are the axial and tangential components of velocity. To vary the chemistry a hydrogen content in the fuel mixture was used between $X_{H_2,fu} = 0$–70%-Vol.

In the experiments both input and output data were measured on premixed swirling flames, i.e. turbulence and reaction rate density data as well the acoustic intensity emitted from the flame.

The acoustical measurement was performed with a G.R.A.S. 40 AK 1/2 in intensity probe located at $r_{\mathrm{mic}} = 0.7$ m which is in the far field with respect to the flame size of 0.06 m and the considered frequency range. Since an anechoic chamber was not available room damping measures were taken to optimize the measurement conditions. Still the measured spectra were distorted by inevitable room acoustics. Therefore a calibration procedure was devised to determine the transfer function of the room. For this a broadband source positioned in place of the flame was measured with the same setup in the laboratory and outside on the lawn. Given the identity of the sources a spectral room transfer function $G(f)$ could be determined, which is used to correct the noise spectra measured in the laboratory. Figure 2 shows a raw noise intensity spectrum and the transfer function $G(f)$. For low frequencies the amplitude variations correspond to modes of the room and are corrected with the corresponding complementary transfer function values. At large frequencies interferences

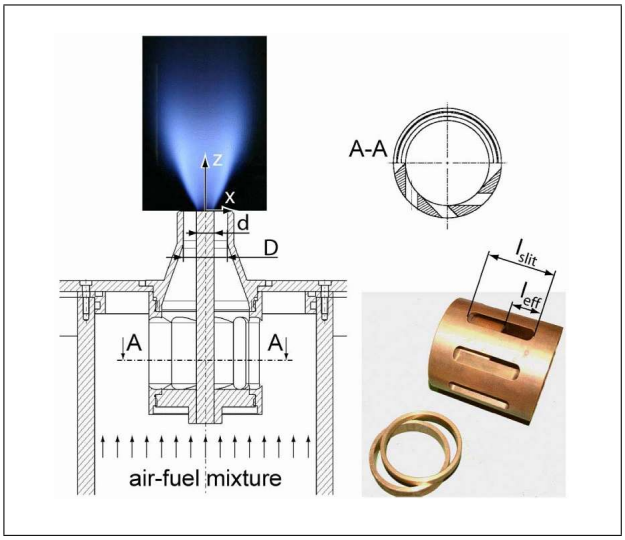


Figure 1. Sketch of the generic swirl burner with flame.

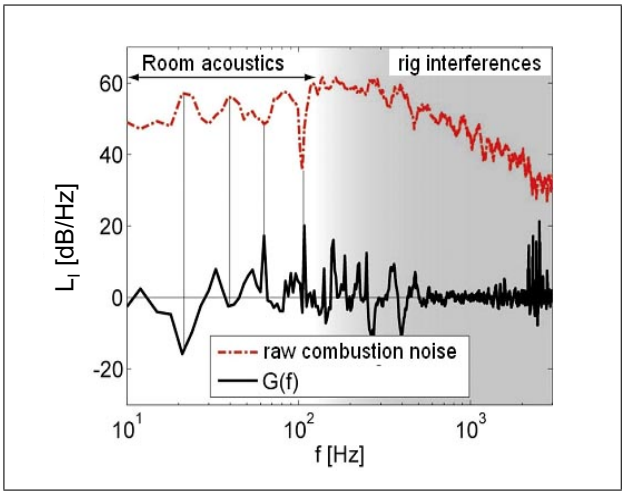


Figure 2. Raw noise intensity spectrum and room transfer function.

of direct waves and waves reflected on the test rig surface occur, which are also seen to be captured by the transfer function. Like this the influence of room acoustics could be greatly reduced.

In spite of all efforts some data scatter has to be accepted in the measurements. In Figure 3 a set of microphone spectra is shown for reproductions the same nominal operating point. While the total sound power of $L_W = 87.3 \pm 0.6$ dB is rather stable, there is a significant variation both in frequency and amplitude. In peak frequency this example shows deviations of ±25% and in some parts of the spectrum a factor 2 in sound power level may occur.

Mean reaction rate density was obtained from deconvoluted pictures of OH^* and CH^* chemiluminescense. Figure 4 shows the burner exit with a typical PIV shot of the flame on the right side. As is indicated with the sketch on the left, the growth of the outer shear layer will influence the flame stoichiometry by providing transport and mixing of ambient air to the fresh gas. Since no flame burns

Document downloaded by @DAEL, 2026-11-19 23:02:43 - personal use only

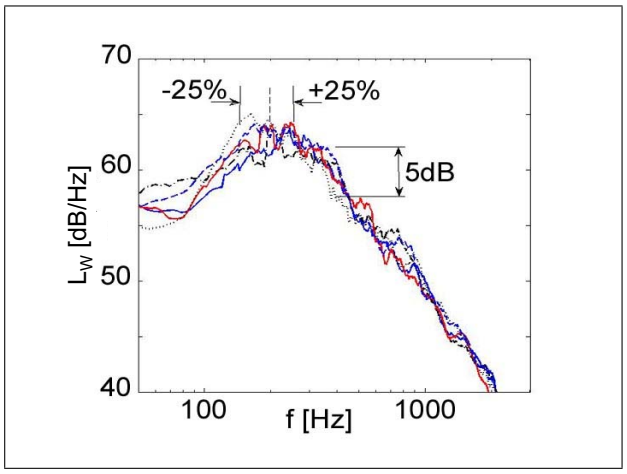


Figure 3. Reproducibility of microphone spectra.

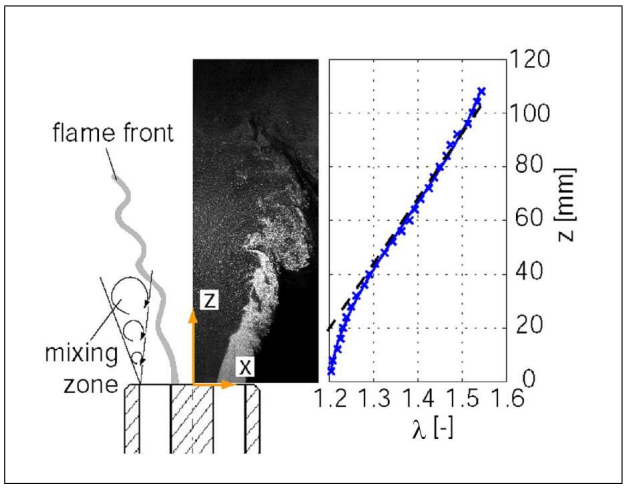


Figure 4. Left: PIV shot of the flame at $\Phi = 0.83$. Right: Air excess ratio ($\lambda = 1/\Phi$) over distance.

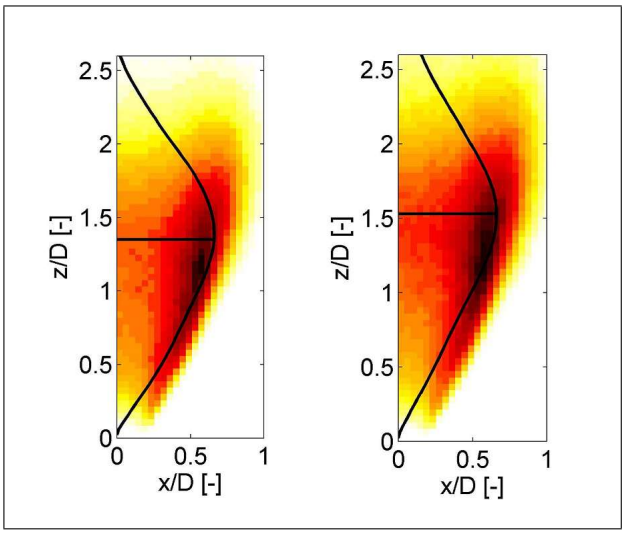


Figure 5. Planar distribution of OH^* chemiluminescense. Left: Original data. Right: Air excess corrected data. Lines indicate the axial intensity distribution.

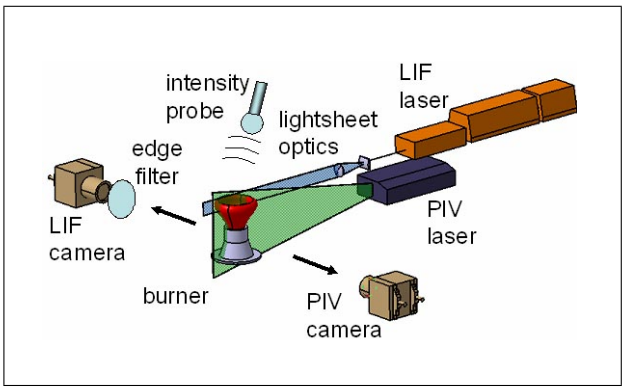


Figure 6. Sketch of the experimental setup.

in the outer shear layer also transport of fresh mixture to the outside takes place which shows in the picture as a rather fuzzy texture. On the inside the flame burns as is seen by the sharp contrast in particle density. As the outer shear layer takes influence, also the inner boundary becomes more distorted as the reaction kinetics are changed reducing the flame speed. Therefore a correction for the entrainment of ambient air is necessary as the air excess deviates significantly from the nominal value at the burner exit. This is done with the method proposed by Wäsle *et al.* [22] and described in detail in [21]. It is based on the spectral analysis of the relative intensities of the OH^* and CH^* chemiluminescense along the axis of the flame that can be used to determine the air excess as a function of axial distance. Using a calibration table obtained from an enclosed flame with constant equivalence ratio the intensities can be corrected as a function of axial distance from the burner as is demonstrated in Figure 5.

The deconvolution of the corrected chemiluminescense image uses the very robust algorithm by Dribinski *et al.* [23], which has been further improved with a reverse calibration procedure. It fixes the free parameter of the Dribinski procedure by requiring a least square fit of the original and the re-convoluted image of the deconvoluted frame (see [21]). Given that the integral of heat release density matches the total heat release the local heat release density distribution obtained.

The planar velocity field and the planar distribution of progress variable data were obtained in the meridional plane of the swirling flame applying simultaneously particle imaging velocimetry (PIV) and Laser Induced Fluorescense (LIF) at frame rates of 1 kHz, capturing up to 2048 frames with 1024x1024 pixels per set. Since the whole flame was captured, the image resolution was typically 0.05 mm/pixel. The PIV analysis requires an interrogation kernel of 32×32, such that the velocity field was resolved in steps of 1.7 mm. As can be seen in Figure 6 two laser light sheets have been interlaced, such that the 283 nm/80 µJ IF-laser pulse illuminates the plane between the two 527 nm/10 mJ PIV-laser shots. To separate the LIF response from the seeding particle Mie diffraction also created by the LIF laser pulse, an edge filter was used.

Document downloaded by @DAEL, 2026-11-19 23:02:43 - personal use only

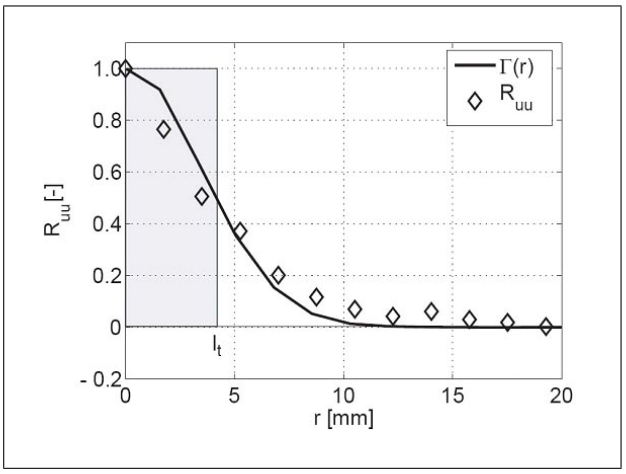


Figure 7. Principle of integral scale determination using a regression fit.

As the signal to noise ratio of the LIF pictures is fairly low, they need to be post processed before they can be used for analysis. This is done in three steps. First the overall intensity distribution of the light sheet is corrected by calculating the vertical integral intensity distribution which is then used to scale the lines. Secondly for very noisy pictures a gamma-correction filter [24] is applied which reduces noise. Though the filter is non- linear its effect on the finally binarized picture was small apart from reducing artificial features due to noise. In most cases this filter was not necessary. Thirdly the flame front is enhanced using a high-pass filter on a 3x3 kernel. Given that the velocity field is resolved only on a length scale larger than laminar flame thickness and considering the influence of filtering, the LIF data is finally binarized with a threshold value, such that the result is the momentary flame front position.

For the extraction of the integral turbulence length scales of velocity and progress variable it showed that the use of a regression fit of the cross correlation function with a gaussian model as proposed by Boineau *et al.* [10] and shown in Figure 7 gave the best reproducible and physically most plausible results.

As proposed in Winklers thesis [25] the PIV-LIF data also allows to evaluate the local mean heat release rate using the Schmid-model given in equation (5) and the entrainment correction to obtain the local values of the mixture. Figure 8 shows the comparison of radial distributions of mean heat release rate as determined from chemiluminescense and from PIV-LIF data using the Schmid-model. Both methods agree qualitatively however in the region close to the burner exit, $z/D = 0.5$, the Schmid model results in higher mean heat release rate density and downstream at $z/D = 2$ the distribution determined from chemiluminescense is shifted radially further out.

The 1-D progress variable spectrum was calculated from the Fourier-transformed correlation coefficient of progress variable [25].

$$E_1(\kappa_1, t) = \int_{-\inf}^{\inf} R_{cc}(x, t)\, \mathrm{e}^{-\mathrm{i}\kappa_1 x}\, \mathrm{d}x. \tag{12}$$

Assuming isotropic turbulence the three dimensional spectrum results [26],

$$E(\kappa_1, t) = -\kappa_1 \frac{\partial E_1(\kappa_1, t)}{\partial \kappa_1}. \tag{13}$$

To qualify the underlying reaction model by Schmid [27, 19] the scalar dissipation of progress variable was determined from the balance equation of progress variable variance $\widetilde{c'^2}$ for a non-swirling case using the simultaneous PIV-LIF data [25]. After simplifications Winkler obtains the following expression to determine the scalar dissipation rate $\epsilon_{c,SD}$ from the simultaneous PIV-LIF-data,

$$\begin{aligned} 2\bar{\rho}\epsilon_{c,SD} \;=\; & -2\bar{\rho}\left(\widetilde{v_r' c'}\frac{\partial \bar{c}}{\partial r} + \widetilde{v_z' c'}\frac{\partial \bar{c}}{\partial z}\right) \\ & - 2\bar{\rho}\left(\tilde{v}_r \frac{\partial \widetilde{c'^2}}{\partial r} + \tilde{v}_z \frac{\partial \widetilde{c'^2}}{\partial z}\right) \\ & - \left(\frac{1}{r}\frac{r\bar{\rho}\widetilde{v_r' c'^2}}{\partial r} + \frac{\bar{\rho}\widetilde{v_z' c'^2}}{\partial z}\right). \end{aligned} \tag{14}$$

The model based scalar dissipation rate $\epsilon_{c,MB}$ is obtained equation (1) applying the Schmid model,

$$\epsilon_{c,MB} = C_D \frac{C_s C_D}{\alpha}\frac{1}{\tau_t} \cdot \tilde{c}\left(1 - \tilde{c}\right). \tag{15}$$

All expressions in equations (14) and (15) can be obtained from the PIV-LIV data, such that a direct qualification of the model is possible. Also the amplitude scaling function C_s can be evaluated using equation (15) and inserting the scalar dissipation obtained from equation (14).

$$C_s = \tau_t \frac{\alpha}{C_D^2\, \tilde{c}\left(1 - \tilde{c}\right)} \cdot \epsilon_{c,SD}. \tag{16}$$

4. Results and discussion

In this section first the key components of the model are analyzed, before the overall comparison between predicted and measured pressure spectra is shown. Finally two examples of the model application are given.

4.1. Length scales and the wavenumber spectrum

The modeling of the spatial spectrum of progress variable by the normalized kinetic energy spectrum in equation (3) implies the proportionality between the scales of turbulent velocity fluctuations and those of progress variable. In Figure 9 the integral length scales of progress variable and velocity are compared over the distance from the burner exit. It is seen that within the experimental uncertainty both scales are proportional with a factor of 1.6. This factor is the result of the Damköhler number influence, that is expected from equation (9). For $u'/s_l > 1$ and $\delta_l/l_t \approx a_0/(s_l \cdot l_t) << 1$ there results

$$\frac{l_t}{l_c} = \frac{1}{C_\tau \cdot \left(1 + Da_t^{-2}\right)^{0.25}}. \tag{17}$$

Document downloaded by @DAEL, 2026-11-19 23:02:43 - personal use only

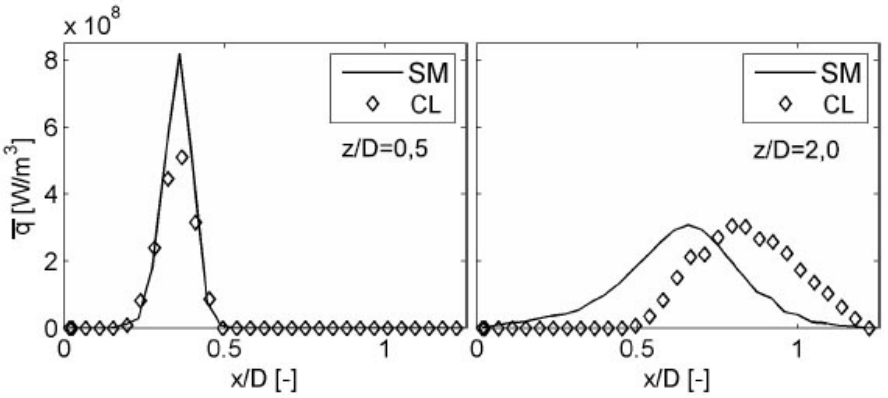


Figure 8. Comparison of mean heat release rate determined from chemiluminescense data (CL) and from PIV-LIF data using the Schmid model (SM).

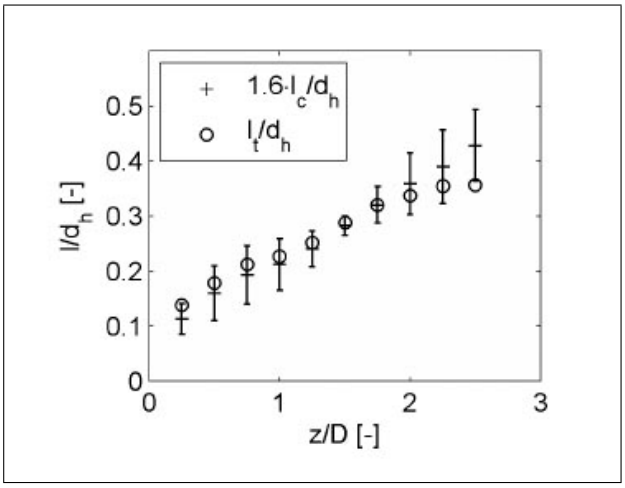


Figure 9. Comparison of turbulence length scale l_t and progress variable length scale l_c for $S = 0.54$, $\dot{Q}_{th} = 60$kW and $\phi = 0.83$ as a function of burner distance.

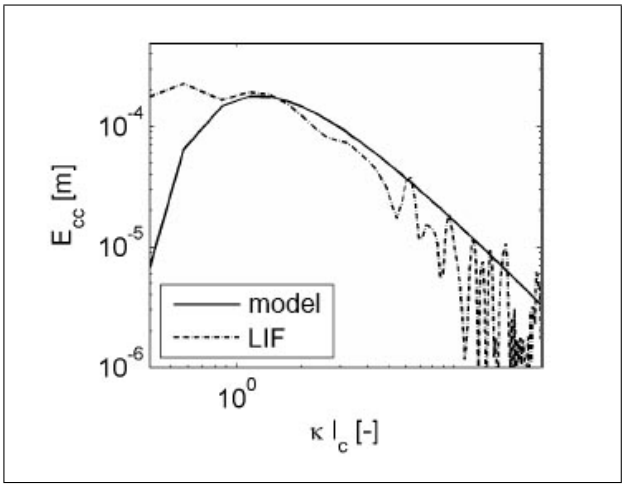


Figure 11. Comparison of measured and modeled progress variable spectrum at $z/D = 1.25$ for $S = 0.54$, $\dot{Q}_{th} = 60$ kW and $\phi = 0.83$.

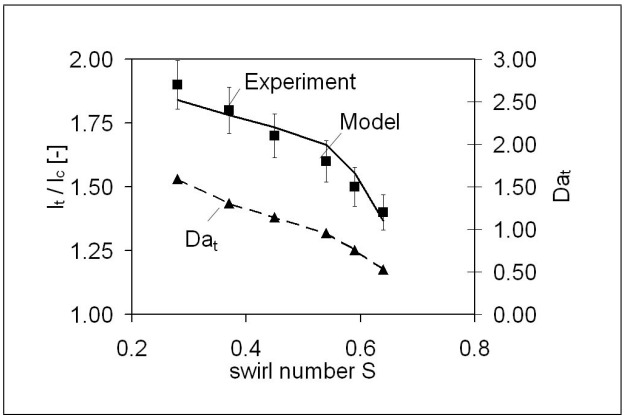


Figure 10. Scaling coefficient of l_t/l_c. Comparison of model and experiment for different swirl numbers at $\dot{Q}_{th} = 60$kW and $\phi = 0.83$.

In Figure 10 the scaling factors determined experimentally are compared with the result of equation (17) for a constant power and equivalence ratio varying the swirl strength. With all other parameters fixed this corresponds to a variation of Damköhler number as shown in the dashed line. The comparison of model spectrum and measured spectrum evaluated from the PIV-LIV dataset at a fixed location according to equations (12) and (13) is shown in Figure 11. The comparison is very good but for the low wavenumber range which is dominated by the particular flow geometry and as such non-universal [28]. The same quality of comparison was also found at all other locations.

4.2. Scalar dissipation model and the amplitude scaling

The coupling between the dissipation rates of turbulence velocity fluctuations and progress variable varies depending on the ratio of time scales, i.e. Damköhler number. This is modeled using the Schmid model. The PIV-LIF data was analyzed given by equations (14) and (15) at different positions in the flame, which were chosen to provide a large variation of turbulent Reynolds and Damköhler number. The comparison is shown in Figure 12, where the lines show the dissipation rate $\epsilon_{c,MB}$ given by the Schmid model according to equation (15) and the symbols denote the data obtained from the balance equation of progress

Document downloaded by @DAEL, 2026-11-19 23:02:43 - personal use only

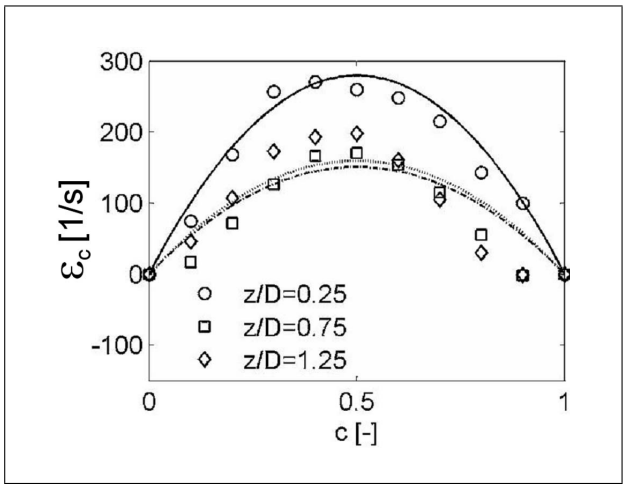


Figure 12. Comparison of scalar dissipation rates determined from balance equation (14)(symbols) and from the Schmid model (lines) at three burner distances for $S = 0.54$, $\dot{Q}_{th} = 60$kW and $\phi = 0.91$.

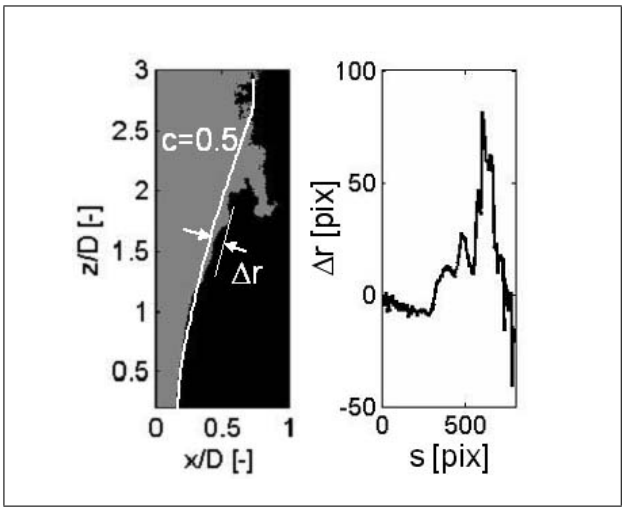


Figure 14. Left: Instantaneous LIF picture showing the $\tilde{c} = 0.5$ line with the normal excursion of the momentary front. Right: Local excursion along the $\tilde{c} = 0.5$ line.

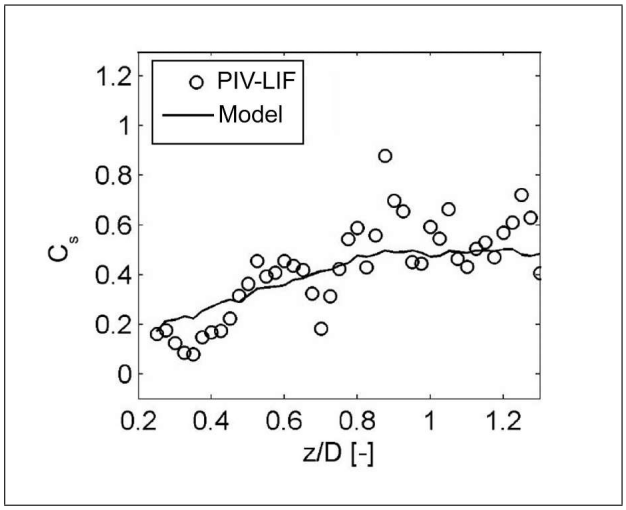


Figure 13. Comparison of amplitude scaling function C_s from equation (16) (symbols) and from the Schmid model 7 (lines) at three burner distances for $S = 0.54$, $\dot{Q}_{th} = 60$kW and $\phi = 0.91$.

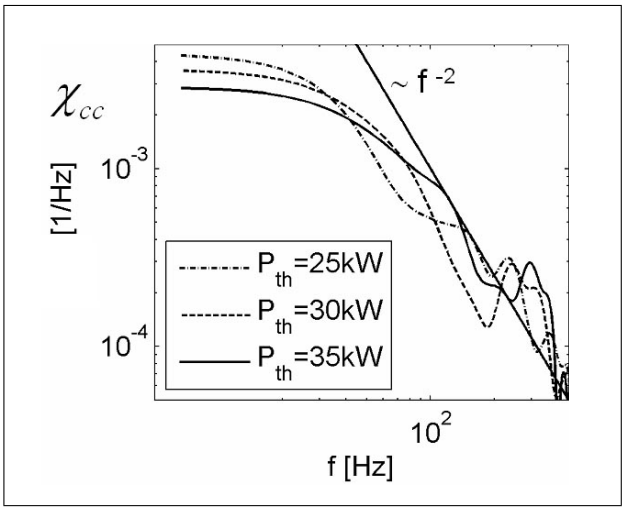


Figure 15. Lagrange spectra ψ_{cc} of progress variable in a stoichiometric, non-swirling flame.

variable variance. Very good comparison both at the root of the flame with small Damköhler number and at the tip, where the dissipation rate is close to the high Damköhler number limit, confirm the chosen modeling strategy.

The comparison in Figure 13 between the scaling function C_s determined from $\epsilon_{c,SD}$ and from the Schmid model is good if one accepts the larger data scatter in the values determined from the balance equation of $\widetilde{c'^2}$. There seems to be an oscillatory behavior in the data points. This was seen similarly for very different operating points and probably reflects finite transform effects.

4.3. Spatial-temporal mapping

The mapping between wavenumber and frequency in equation (8) is a corner stone of the model which was investigated in more detail by Winkler [25, 29] on a non-swirling flame. He determined Lagrange time correlations along the $\tilde{c} = 0.5$ line as sketched in Figure 14. The local excursions of the momentary flame front relative to the $\tilde{c} = 0.5$ line were calculated for each picture of the 2048 frame sequence. Next the resulting $\Delta r - s$-patterns were cross correlated between successive pictures which provides the Lagrange correlation coefficient and with the Fourier-transform the frequency spectrum. Given that the scaling of equation (8) holds, the inertial range $\kappa^{-5/3}$ scaling in the wavenumber domain will correspond with a f^{-2} behavior in the frequency range.

As can be seen from Figure 15 the measured spectra follow the f^{-2} scaling fairly well, confirming the assumed wavenumber-frequency mapping.

4.4. Global comparison

An extensive study was performed to assess the predictive capability of the model [21] varying power, equivalence ratio, fuel composition and swirl intensity.

Document downloaded by @DAEL, 2026-11-19 23:02:43 - personal use only

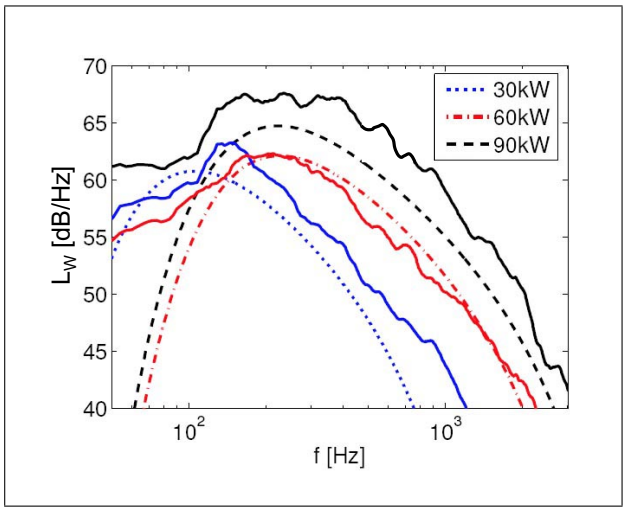


Figure 16. Comparison of modeled (broken) and measured (solid) noise spectra. Variation of power at $\phi = 0.83$, $S = 0.54$ with natural gas.

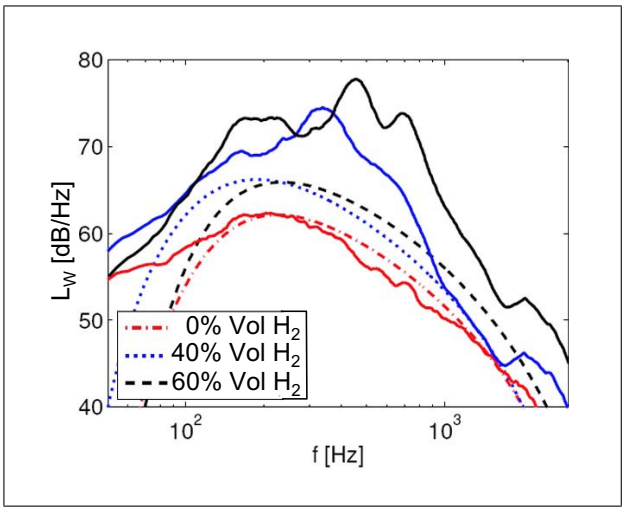


Figure 18. Comparison of modeled (broken) and measured (solid) noise spectra using chemiluminescense data. Variation of fuel mixture at $\dot{Q}_{th} = 60kW$, $S = 0.54$, $\phi = 0.83$.

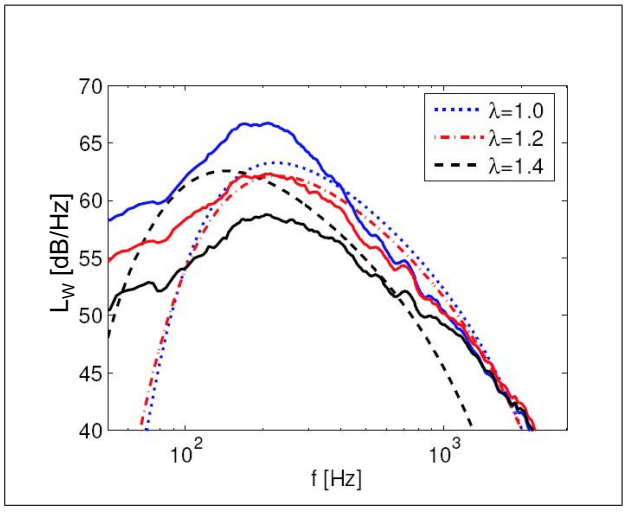


Figure 17. Comparison of modeled (broken) and measured (solid) noise spectra. Variation of air excess at $\dot{Q}_{th} = 60kW$, $S = 0.54$.

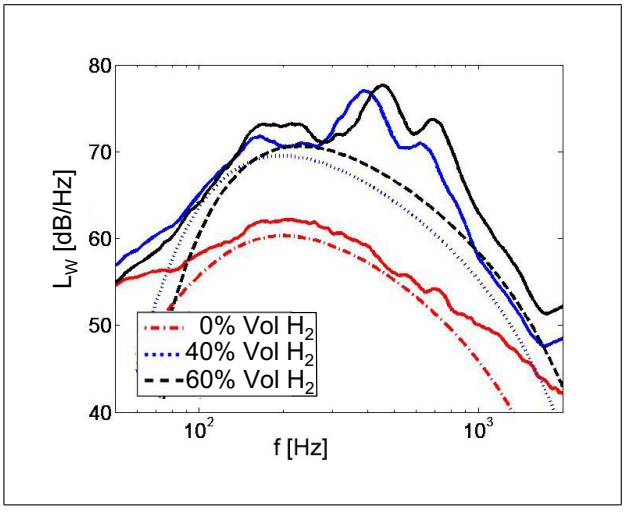


Figure 19. Comparison of modeled (broken) and measured (solid) noise spectra using PIV-LIF-data. Variation of fuel mixture at $\dot{Q}_{th} = 60kW$, $S = 0.54$, $\phi = 0.83$.

In Figure 16 the comparison between measured and modeled noise spectra is shown for the variation of power. For the high power cases, the correspondence between model and measurement is very good. The model captures the amplitude and the shift in frequency. Towards high power, the effect of the chemical time scale reduces the fluctuation of progress variable such that the increase of peak amplitude is reduced. At low power the amplitude is significantly under predicted while the frequency range is still captured fairly well. In this case the assumption of $u'/s_l \gg 1$ is not warranted anymore and, as Winkler [25] discusses, the effect of local acceleration due to the density gradient affects the direct proportionality between velocity and progress variable fluctuation.

The variation of fuel composition was performed by adding up to 60%-Vol of hydrogen to the fuel while keeping the flame temperature constant. Figure 18 presents the results using chemiluminescense data to obtain the mean heat release rate density, whereas in Figure 19 the heat release rate density is obtained from PIV-LIF-data using the Schmid model. With hydrogen, a significant reduction in flame length is observed, such that the local power density increases strongly for constant total power. This causes an increase in the peak amplitude. The reduction in flame length corresponds with smaller length scales which is seen as a shift towards higher frequencies. At the same time the faster chemistry increases the Gibson scale which creates a steeper spectral fall off. The model captures these effects very well, which indicates that the underlying Schmid model captures the influence of the fuel chemistry. Wäsle [21] showed, that the measured amplitude peaks seen with hydrogen addition for intermediate frequencies can be attributed to resonance in the burner nozzle. Comparing Figures 18 and 19 the model quality

Document downloaded by @DAEL, 2026-11-19 23:02:43 - personal use only

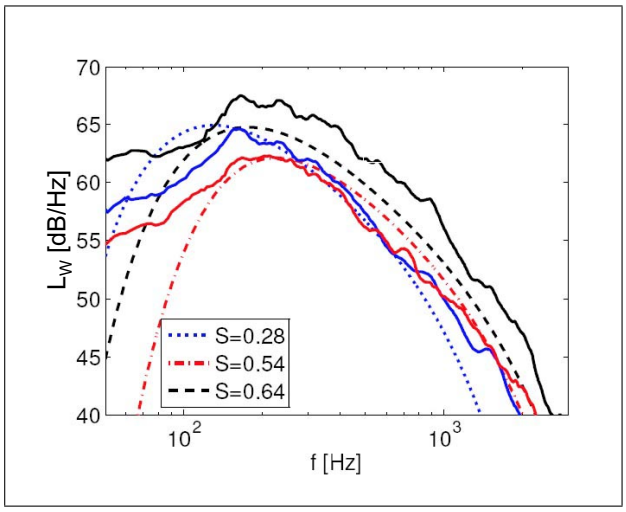


Figure 20. Comparison of modeled (broken) and measured (solid) noise spectra. Variation of swirl number at $\dot{Q}_{th} = 60kW$, $\phi = 0.83$.

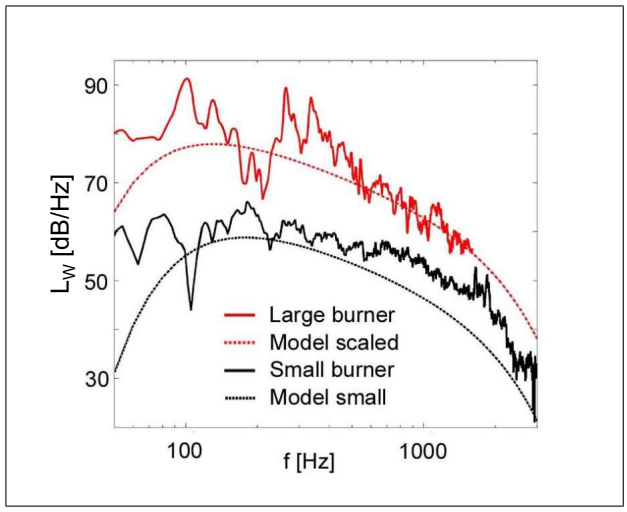


Figure 21. Application of the model for scaling. Large burner data by Bender [30].

improves using the PIV-LIF data, which indicates the importance of the proper heat release rate density for the predictive capability of the model.

The influence of air excess, $\lambda = 1/\phi$, is shown in Figure 17. Here the experiments display a significant change in peak amplitude at essentially the same frequency. On the contrary the model results give a change of peak frequency with the lengthening of the flame for increasing air excess but the peak amplitude remains essentially constant. As Wäsle [21] discusses this is probably due to an insufficient correction method of the chemiluminescense that provides the heat release distribution, which is subject to further investigation.

Varying the swirl number as shown in Figure 20 a combination of effects are superimposed. Increasing swirl will shorten the flame and thus increase power density, i.e. peak amplitude. With increasing swirl also the entrainment increases which will affect the chemical time scale as well. Like this the lowest and the highest swirl number shown have higher Damköhler numbers of 1.72 and 1.62 respectively, whereas the intermediate case has a lower value $Da_t = 1.4$. As seen before in Figure 10 this corresponds with lower integral scales of the progress variable which in turn reduces the coherence volume and increases the peak frequency. This explains that the intermediate swirl number has a lower peak amplitude at a higher frequency then the other two cases which the model captures very well.

4.5. Practical application

As an example for practical application of the model the scaling of combustion noise spectra between burners is considered. Bender and Büchner [30] presented combustion noise spectra from a premixed swirl burner having two swirlers running at $\dot{Q}_{th} = 320kW$, $\phi = 0.71$. A factor 2 scaled down version was built and measured with $\dot{Q}_{th} = 80kW$ such that the model spectrum could be calculated. Next the coordinates of the small burner field distributions of turbulence and heat release were scaled up by a factor of 2. Also the turbulence length scales were scaled up by a factor of 2 whereas the turbulence velocities were kept as in the case of the small burner. In Figure 21 the measured and calculated results of the small burner as well as the scaled model prediction and the measured large burner spectra are shown. In the small burner case, the model under predicts the acoustical spectrum at higher frequencies which points at difficulties in the resolution of the smaller turbulence scales in the measurement. For the large burner some peaks in the low frequency range occur which Bender and Büchner identify as precessing vortices caused by the inner swirler, which is not present in the small burner. Apart from this the over all spectral distribution is reproduced remarkably well. Comparing the integrated acoustical power scaling of measured 108.8 dB / 94.3 dB = 14.5 dB with the model prediction 106.4 dB / 89.2 dB = 17 dB the model scaling over predicts the total power by 3 dB.

The second example focuses on the application of the model as a post-processing tool for reactive CFD-RANS models. This was previously shown by Hirsch *et al.* [31] for the swirl variation of the premixed jet flame experiment presented above. The calculation was done using an axial symmetrical grid using a user defined Schmid model with the FLUENT V6.1 code. Figure 22 shows the very good comparison between measurement and model.

5. Summary and conclusions

In this paper a model for the prediction of combustion noise spectra based on time mean data of turbulence and heat release rate is analyzed based on four experimental techniques. The acoustical measurement of noise spectra and their correction for room acoustics is described. The method to obtain the distribution of heat release rate based on corrected chemiluminescense is shown. PIV is used to

Document downloaded by @DAEL, 2026-11-19 23:02:43 - personal use only

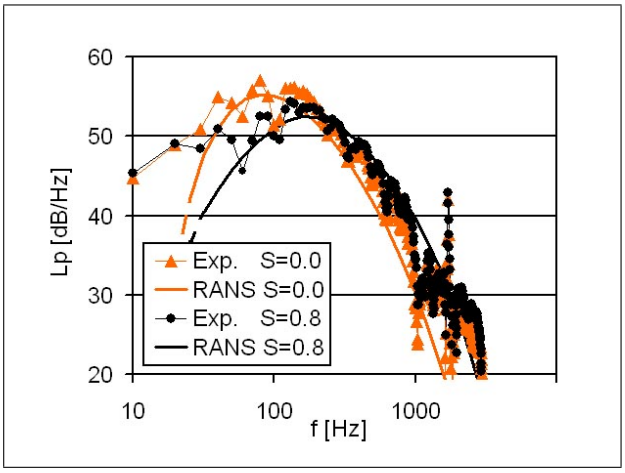


Figure 22. Prediction of combustion noise spectra using reactive CFD-RANS data.

determine the turbulence velocity and length scales. With LIF the flame structure is captured and wavenumber spectra of progress variable are obtained. Combining PIV and LIF in a high speed simultaneous set up Lagrange spectra of the progress variable are calculated. With these methods the sub models are verified with experimental evidence. These are: The calculation of the length scales of progress variable from the turbulent velocity scale and the shape of the wavenumber spectrum. The modeling of the scalar dissipation rate of progress variable and the derived amplitude scaling. The wavenumber frequency mapping by measuring Lagrangian spectra of progress variable. The overall performance of the model is then assessed in a parametric study, varying power, fuel composition, air ratio and swirl. Finally two examples of the application of the model are given, which emphasize its usefulness in the engineering context.

Given the overall good quantitative comparison of the model with measurement we conclude, that the model properly reflects the physics of noise generation in turbulent flames. In particular the amplitude scaling and the wavenumber time mapping unveil the important processes that govern the formation of the noise spectrum. With this insight combustor designers are enabled to systematically optimize the combustion system. The simplicity of the model make it very useful as a post-processing tool that can be used to calculate equivalent source terms for acoustical models to predict noise spectra within combustion chambers. This work is in progress.

Acknowledgements

The authors gratefully acknowledge the financial support by the Bavarian Research Cooperation (FortVer) and the German Research Council (DFG) through the Research Unit FOR486 “Combustion Noise”and the German Federal Ministry for Education and Research under Grant 03STA1AC.

References

[1] M. J. Lighthill: On sound generated aerodynamically. Part I. General theory. Proceedings of the Royal Society of London, Series A. Mathematical and Physical Sciences, London **211** (1952) 564–587.

[2] I. Proudma: The generation of noise by isotropic turbulence. Proceedings of the Royal Society of London, Series A. Mathematical and Physical Sciences, London **214** (1952) 119–132.

[3] H. Ribner: Quadrupole correlation governing the pattern of jet noise. Journal of Fluid Mechanics **38** (1969) 1–24.

[4] T. J. B. Smith, J. K. Kilham: Noise generation by open turbulent flames. Journal of the Acoustical Society of America **35** (1963) 715–724.

[5] W. C. Strahle: On combustion generated noise. Journal of Fluid Mechanics **49** (1971) 399–414.

[6] S. L. Bragg: Combustion noise. Journal of the Institute of Fuel (1963) 12–16.

[7] J. R. Mahan, J. D. Jones: Recovery of burner acoustic source structure from far-field sound spectra. AIAA Journal 63 **22** (1984).

[8] J. Wäsle, A. Winkler, T. Sattelmayer: Spatial coherence of the heat release fluctuations in turbulent jet and swirl flames. Kluwer, Flow Turbulence and Combustion **75** (2005) 29–50.

[9] P. Clavin, E. D. Siggia: Turbulent premixed flames and sound generation. Combustion Science and Technology **78** (1999) 147–155.

[10] P. Boineau, Y. Gervais, V. Morice: An aerothermoacoustic model for computation of sound radiated by turbulent flames. Internoise 96, 1996.

[11] S. A. Klein, J. B. W. Kok: Sound generation by turbulent non-premixed flames. Combustion Science and Technology **149** (1999) 267–295.

[12] S. A. Klein: On the acoustics of turbulent non-premixed flames. PhD thesis, Universiteit Twente, 2000. ISBN 90-36514096.

[13] C. Hirsch, J. Wäsle, A. Winkler, T. Sattelmayer: A spectral model for the sound pressure from turbulent premixed combustion. 31st Int. Symp. (Int.) on Combustion, 2006, 1435–1441.

[14] D. G. Crighton, A. P. Dowling, J. E. Ffowcs Williams, M. Heckl, F. G. Leppington: Modern methods in analytocal acoustics. Springer, London, 1992.

[15] B. Mühlbauer, R. Ewert, O. Kornow, B. Noll, J. W. Delfs, M. Aigner: Simulation of combustion noise using CAA with stochastic sound sources from RANS. 14th AIAA/CEAS Aeroacoustics Conference (29th AIAA Aeroacoustics Conference), Vancouver, British Columbia, 5-7 May 2008.

[16] N. Peters: Turbulent combustion. Cambridge Univ. Press, 2000.

[17] H. Tennekes, J. L. Lumley: A first course in turbulence. The MIT Press, 11th printing 1987, 1972.

[18] R. Borghi: On the structure of turbulent premixed flames. C. Bruno and C. Casci, Pergamon Press, 1984.

[19] H. P. Schmid, P. Habisreuther, W. Leuckel: A model for calculating heat release in premixed turbulent flames. Combustion and Flame **113** (1998) 79–91.

[20] A. Winkler, J. Wäsle, T. Sattelmayer: Experimental inverstigations on the acoustic efficiency of premixed swirl stabi-

Document downloaded by @DAEL, 2026-11-19 23:02:43 - personal use only

lized flames. 11th AIAA/CEAS Aeroacoustics Conference, Monterey, 2005, paper AIAA–2005–2908.

[21] J. G. Wäsle: Vorhersage der Lärmemission turbulenter Vormischflammen. Ph.D. thesis, Lehrstuhl Thermodynamik, Technische Universität München, 2007.

[22] J. A. Wäsle, A. Winkler, M. Lauer, T. Sattelmayer: Combustion noise modeling using chemiluminescence data as indicator for the heat release distribution. European Combustion Meeting, Chania, Greece, 2007.

[23] V. Dribinski, A. Ossadtchi, V. A. Mandelshtam, H. Reisler: Reconstruction of Abel-transformable images: The basis-set expansion Abel transform method. Review of Scientific Instruments **73** (2002) iss. no. 7.

[24] R. C. Gonzales, P. Wintz: Digital image processing. 2nd edition. Addison-Wesley Publishing Company, 1987.

[25] A. Winkler: Validierung eines Modells zur Vorhersage turbulenten Verbrennungslärms. Ph.D. thesis, Lehrstuhl Thermodynamik, Technische Universität München, 2007.

[26] J. O. Hinze, B. J. Clark: Turbulence. 2nd edition. McGraw-Hill, 1959.

[27] H. P. Schmid: Ein Verbrennungsmodell zur Beschreibung der Wärmefreisetzung von vorgemischten turbulenten Flammen. Ph.D. thesis, Engler-Bunte-Institut, Universität Karlsruhe (TH), 1995.

[28] N. Peters: A spectral closure for premixed turbulent. Combustion in the Flamelet Regime **J. Fluid Mech.** (242) 1992.

[29] A. Winkler, J. A. Wäsle, T. Sattelmayer: Development of a HS-LIF-system for Lagrangian correlation measurement. Experiments in Fluids (2008) submitted.

[30] C. Bender, H. Büchner: Noise emissions from a premixed swirl combustor. 12th International Congress on Sound and Vibration, Lisbon, Portugal, 2005.

[31] C. Hirsch, A. Winkler, J. A. Wäsle, T. Sattelmayer: Calculating the turbulent noise source of premixed swirl flames from time mean reactive rans variables. 13th International Congress on Sound and Vibration, Vienna, Austria, 2006.

Document downloaded by @DAEL, 2026-11-19 23:02:43 - personal use only